Ketene–Ketene Rearrangement: Substituent Effects on the 1,3-Migration in α-Oxo Ketenes

Ming Wah Wong* and Curt Wentrup*

Department of Chemistry, The University of Queensland, Brisbane, Queensland 4072, Australia

Received April 27, 1994®

The mechanism of the 1,3 migration in a series of α-oxo ketenes, RCOCH=C=O (R = H, CH_3, NH_2, OH, SH, SiH_3, OCH_3, SCH_3, $N(CH_3)_2$, and C_6H_5), was studied by high-level ab initio molecular orbital calculations up to the QCISD(T)/6-311+G(2d,p) + ZPVE level of theory. The oxo ketene–oxo ketene rearrangement is predicted to proceed via a four-membered cyclic transition structure. The calculated activation barrier depends strongly on the nature of the migrating group (R), ranging from 20 to 200 kJ mol^{-1}. *n*-Electron donor substituents (e.g., NH_2 and SH) are found to stabilize the four-centered transition structures. For the dimethylamino substituent, the 1,3-shift is predicted to be a facile process (barrier = 20 kJ mol^{-1}), and a stable four-membered cyclic interemediate is found to exist on the reaction profile. The predicted 1,3-migratory aptitude is in the order $N(CH_3)_2$ > SCH_3 > SH > NH_2 > OCH_3 > OH > SiH_3 > H > C_6H_5 > CH_3. This calculated trend is consistent with experimental observations. The stabilization of the transition structure can be rationalized by the donor–acceptor interaction between an appropriate *n*- or π-electron donor substituent and the vacant carbon p orbital of the ketene LUMO. The *E*/*Z* conformational preferences (gas phase and solution), rotational barriers, and IR spectra of α-oxo ketenes are also reported.

Introduction

There has been considerable recent interest in the chemistry of α-oxo ketenes.[1,2] These reactive species are important building blocks in organic synthesis, via nucleophilic additions and [4 + 2] cycloadditions, and they undergo a number of unusual rearrangements. In a ^{13}C labeling study, Wentrup and Netsch have shown that benzoylketene can undergo a thermal oxo ketene–oxo ketene rearrangement involving a 1,3-shift of an aryl group (eq 1, R = C_6H_5).[3] Subsequent work indicated that

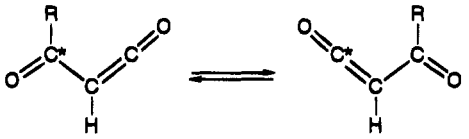

(1)

the imine analogues are also capable of this intriguing 1,3-migration, interconverting imidoylketenes and oxo ketenimines (eq 2).[4] In particular, the rate of the 1,3-migration reaction is found to be strongly dependent on

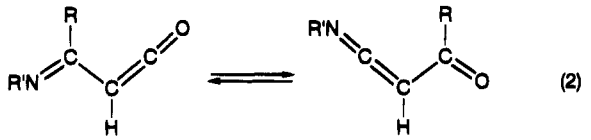

(2)

the nature of the substituent: for the electron rich methylthio (SCH_3) or dimethylamino ($N(CH_3)_2$) group, there is a dramatic acceleration of this rearrangement,[4b,c] while for the methyl substituent the reaction does not take place even under FVP conditions up to 1000 °C.[5] It is also of interest to note the related interconversion of thioacyl isocyanates and acyl isothiocyanates (eq 3),[6] as well as the isomerization of a guanyl isocyanate to a carbamoyl carbodiimide (eq 4), both discovered by Goerdeler et al.[7,8]

The simplest model for the oxo ketene–oxo ketene rearrangement, formylketene (eq 1, R = H), has been studied by ab initio calculations.[9] The calculations

® Abstract published in *Advance ACS Abstracts,* August 1, 1994.

(1) (a) Leung-Toung, R.; Wentrup, C. *Tetrahedron* **1992**, *48*, 7641. (b) Kappe, C. O.; Färber, G.; Wentrup, C.; Kollenz, G. *J. Org. Chem.* **1992**, *57*, 7078. (c) Andreichikov, Y. S.; Kollenz, G.; Kappe, C. O.; Leung-Toung, R.; Wentrup, C. *Acta Chem. Scand.* **1992**, *46*, 683. (d) Leung-Toung, R.; Wentrup, C. *J. Org. Chem.* **1992**, *57*, 4851. (e) Freiermuth, B.; Wentrup, C. *J. Org. Chem.* **1991**, *56*, 2286. (f) Kappe, C. O.; Evans, R. A.; Kennard, C. H. L.; Wentrup, C. *J. Am. Chem. Soc.* **1991**, *113*, 4234. (g) Maier, G.; Reisenauer, H. P.; Sayrac, T. *Chem. Ber.* **1982**, *115*, 2191.

(2) For examples, see: (a) Allen, A. D.; McAllister, M. A.; Tidwell, T. T. *Tetrahedron Lett.* **1993**, *34*, 1095. (b) Coleman, R. S.; Fraser, J. R. *J. Org. Chem.* **1993**, *58*, 385. (c) Chen, C.; Quinn, E. K.; Olmstead, M. M.; Kurth, M. J. *J. Org. Chem.* **1993**, *58*, 5011. (d) Allen, A. D.; Andraos, J.; Kresge, A. J.; McAllister, M. A.; Tidwell, T. T. *J. Am. Chem. Soc.* **1992**, *114*, 1878. (e) Emerson, D. W.; Titus, R. L.; Gonzales, R. M. *J. Org. Chem.* **1991**, *56*, 5301. (f) Witzeman, J. S. *Tetrahedron Lett.* **1990**, *31*, 1401. (g) Kaneko, C.; Sato, M.; Sakaki, J.-J.; Abe, Y. *J. Heterocycl. Chem.* **1990**, *27*, 25. (h) Clemens, R. J.; Witzeman, J. S. *J. Am. Chem. Soc.* **1989**, *111*, 2186. (i) Andreichikov, O. V.; Vinokurova, O. V.; Gein, V. L. *J. Org. Chem. USSR* **1989**, *25*, 2189. (j) Boeckman, R. K., Jr.; Pruitt, J. R. *J. Am. Chem. Soc.* **1989**, *111*, 8286.

(3) (a) Wentrup, C.; Netsch, K.-P. *Angew. Chem., Int. Ed. Engl.* **1984**, *23*, 802. (b) Wentrup, C.; Winter, H.-W.; Gross, G.; Netsch, K.-P.; Kollenz, G.; Ott, W.; Biedermann, G. *Angew. Chem., Int. Ed. Engl.* **1984**, *23*, 800.

(4) (a) Netsch, K.-P. Ph.D. Thesis, University of Marburg, Germany, 1985. (b) Ben Cheikh, A.; Chuche, J.; Manisse, N.; Pommelet, J. C.; Netsch, K.-P.; Lorencak, P.; Wentrup, C. *J. Org. Chem.* **1991**, *56*, 970. (c) Kappe, C. O.; Kollenz, G., Leung-Toung, R.; Wentrup, C. *J. Chem. Soc., Chem. Commun.* **1992**, 487.

(5) Sankar, I. V.; McCluskey, A.; Wentrup, C. Unpublished. Methyl acetoacetate-3-^{13}C (carbonyl labeled) was subjected to flash vacuum pyrolysis at temperatures between 700 and 1100 °C (6×10^{-4} mbar), with product isolation for IR spectroscopy at 77 K (neat). The carbonyl-^{13}C labeled acetylketene, $CH_3{}^{13}COCH{=}C{=}O$, appeared at 2143 cm^{-1}, and the satellite due to natural abundance ^{13}C in the ketene function was detectable at 2090 cm^{-1}. There was no measurable increase in the relative intensity of the latter peak on using FVP temperatures up to 1100 °C, but the ketene decomposed above 1000 °C.

(6) (a) Goerdeler, J.; Jonas, G. *Chem. Ber.* **1966**, *99*, 3572. The migratory aptitudes given for the reaction in eq 3 are $(Alk)_2N$, Alk-(Ar)N > ArS > AlkS ≫ ArO > AlkO. (b) Goerdeler, J.; Wobig, D. *Liebigs Ann. Chem.* **1970**, *731*, 120. (c) Goerdeler, J.; Bartsch, H.-J. *Chem. Ber.* **1985**, *118*, 2294, 4196.

(7) Goerdeler, J.; Raddatz, S. *Chem. Ber.* **1980**, *113*, 1095.

(8) The 1,3-shift of a dimethylamino group in a methylallene, converting a substituted 4-(dimethylamino)buta-1,2-diene to a 2-(dimethylamino)buta-1,3-diene, quantitatively at 80 °C, may also be considered in this context: Mageswaran, S.; Ollis, W. D.; Southam, D. A.; Sutherland, I. O.; Thebtaranonth, Y. *J. Chem. Soc., Perkin Trans. 1* **1981**, 1969.

(9) Nguyen, M. T.; Ha, T.-K.; More O'Ferrall, R. A. *J. Org. Chem.* **1990**, *55*, 3251.

0022-3263/94/1959-5279$04.50/0

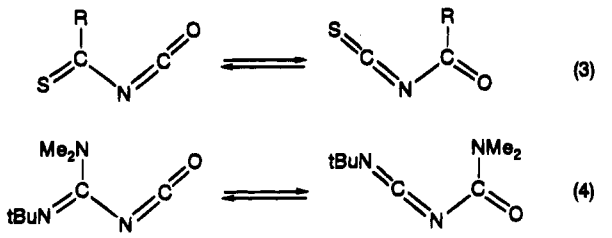

(3)

(4)

indicated that the 1,3-hydrogen shift in formylketene requires a significant activation barrier of 166 kJ mol^{-1}. In order to gain further insight into the mechanism of this intriguing rearrangement process, in particular the influence of substituents on the transition structures, we have undertaken a systematic theoretical investigation of a series of acyl-substituted α-oxo ketenes, RCO-CH=C=O **1**–**10** (R = H, CH_3, NH_2, OH, SiH_3, SH, OCH_3, SCH_3, $N(CH_3)_2$, and C_6H_5) (Chart 1), using high-level ab initio calculations. The calculated trend in activation barriers is in good accord with the experimental observations.[2-6] The origin of the rate acceleration caused by electron rich substituents can be traced to a favorable donor–acceptor interaction between the *n*-electron donor substituent and a vacant carbon p orbital of the ketene LUMO. Further studies will be concerned with the related imidoylketenes, oxoketenimines, vinylketenes, thioacylthioketenes, and other systems.

Chart 1

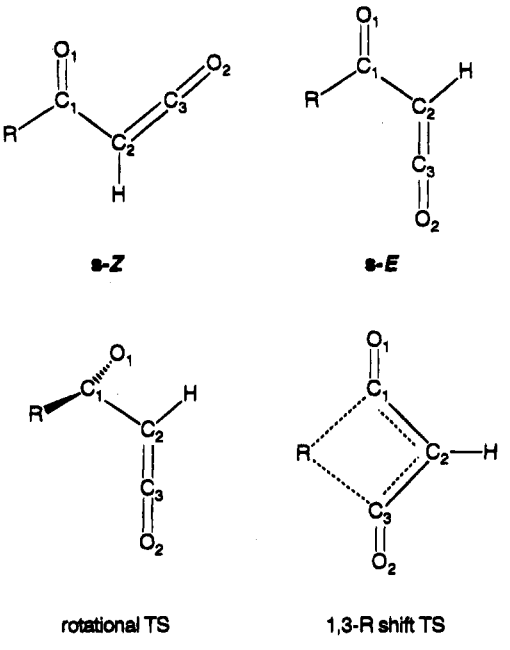

R = H (**1**), CH_3 (**2**), NH_2 (**3**), OH (**4**), SiH_3 (**5**), SH (**6**), OCH_3 (**7**), SCH_3 (**8**), $N(CH_3)_2$ (**9**) and C_6H_5 (**10**)

Computational Method and Results

Standard ab initio molecular orbital calculations[10] were carried out with the GAUSSIAN 92[11] system of programs. Geometry optimizations of *s-Z* and *s-E* forms of α-oxo ketenes and transition structures for *E/Z* isomerization and 1,3-R migration (Chart 1), were performed with the standard polarized split-valence 6-31G* basis set[10] at the Hartree–Fock (HF) and second-order Møller–Plesset perturbation (MP2) levels.[10] Harmonic vibrational frequencies were calculated at the HF/6-31G* level in order to characterize the stationary points as minima and saddle points and to evaluate zero-point vibrational energies (ZPVEs). The directly calculated frequencies and ZPVEs were scaled by 0.8929 and 0.9135, respectively, to account for the overestimation of vibrational frequencies and ZPVEs at this level of theory.[12] Improved relative energies were obtained through quadratic configuration interaction with single, double, and augmented triple [QCISD(T)][13] calculations with the larger 6-311+G(2d,p)[8] basis set, based on the MP2(full)/6-31G* optimized geometries. This level of theory is evaluated with the use of the additivity approximation

$$\Delta E(\text{QCISD(T)/6-311+G(2d,p)}) = \Delta E(\text{QCISD(T)/6-31G*}) - \Delta E(\text{MP2/6-31G*}) + \Delta E(\text{MP2/6-311+G(2d,p)}) \quad (5)$$

Our best relative energies discussed below correspond to QCISD(T)/6-311+G(2d,p) values with zero-point vibrational contributions. Unless otherwise noted, these are the values referred to in the text. To provide an estimate of the likely accuracy of our computed relative energies at the QCISD(T)/6-311+G(2d,p) + ZPVE level, we have determined also the relative energies of the parent compound, formylketene (**1**) using the G2(MP2) level of theory[14] (corresponding effectively to QCISD(T)/6-311+G-(3df,2p) level with zero-point vibrational and isogyric corrections). The calculated G2(MP2) *E/Z* energy difference, rotational barrier, and 1,3-hydrogen migration barrier for formylketene (**1**) are −0.7, 43.7, and 141.6 kJ mol^{-1}, respectively, fairly close to our best estimates (−0.7, 41.4, and 142.0, respectively). This lends confidence to our predicted relative energies for other α-oxo ketenes. For the larger systems, namely, R = OCH_3 (**7**), SCH_3 (**8**), $N(CH_3)_2$ (**9**), and C_6H_5 (**10**), the relative energies were determined at a somewhat lower level of theory, MP3/6-311+G** + ZPVE level, based on the HF/6-31G* optimized geometries. The MP3 energies were also obtained from an additivity approximation:

$$\Delta E(\text{MP3/6-311+G**}) = \Delta E(\text{MP3/6-31G*}) - \Delta E(\text{MP2/6-31G*}) + \Delta E(\text{MP2/6-311+G**}) \quad (6)$$

The frozen-core approximation was employed for all single-point correlated calculations.

The effects of solvents on the *E/Z* isomerism of **1**, **2**, and **4** were studied using the self-consistent reaction field (SCRF) method.[15] In this model the solute is taken to occupy a spherical cavity of radius a_0 which is calculated

(10) Hehre, W. J.; Radom, L.; Schleyer, P. v. R.; Pople, J. A. *Ab Initio Molecular Orbital Theory*; Wiley: New York, 1986.
(11) Frisch, M. J.; Trucks, G. W.; Head-Gordon, M.; Gill, P. M. W.; Wong, M. W.; Foresman, J. B.; Johnson, B. G.; Schlegel, H. B.; Robb, M. A.; Replogle, E. S.; Gomperts, R.; Andres, J. L.; Raghavachari, K.; Binkley, J. S.; Gonzalez, C.; Martin, R. L.; Fox, D. J.; DeFrees, D. J.; Baker, J.; Stewart, J. J. P.; Pople, J. A. *GAUSSIAN 92*, Gaussian Inc.: Pittsburgh, PA, 1992.
(12) Pople, J. A.; Scott, A. P.; Wong, M. W.; Radom, L. *Isr. J. Chem.* **1993**, *33*, 345.
(13) Pople, J. A.; Head-Gordon, M.; Raghavachari, K. *J. Chem. Phys.* **1987**, *87*, 5968.
(14) (a) Curtiss, L. A.; Raghavachari, K.; Pople, J. A. *J. Chem. Phys.* **1993**, *98*, 1293. (b) Curtiss, L. A.; Raghavachari, K.; Trucks, G. W.; Pople, J. A. *J. Chem. Phys.* **1991**, *94*, 7221.
(15) (a) Wong, M. W.; Frisch, M. J.; Wiberg, K. B. *J. Am. Chem. Soc.* **1991**, *113*, 4776. (b) Wong, M. W.; Wiberg, K. B.; Frisch, M. J. *J. Chem. Phys.* **1991**, *89*, 8991.

Table 1. Calculated (MP2/6-31G*) Structural Parameters for Equilibrium and Transition Structures of α-Oxo Ketenes[a]

parameter[b]	H (1)	CH_3 (2)	NH_2 (3)	OH (4)	SH (5)	SiH_3 (6)
			s-Z Conformer			
$r(C_1-O_1)$	1.229	1.232	1.231	1.222	1.224	1.242
$r(R-C_1)$	1.106	1.510	1.376	1.360	1.795	1.920
$r(C_1-C_2)$	1.458	1.469	1.472	1.456	1.459	1.465
$r(C_2-C_3)$	1.335	1.333	1.330	1.332	1.334	1.336
$r(C_2-H)$	1.083	1.083	1.083	1.082	1.083	1.082
$r(C_3-O_2)$	1.169	1.171	1.172	1.171	1.170	1.170
$\angle RC_1O_1$	121.2	122.4	122.5	123.2	122.9	117.5
$\angle O_2C_1C_2$	124.7	122.2	123.0	126.1	124.6	122.4
$\angle C_1C_2C_3$	117.3	116.9	116.5	117.3	116.4	116.6
$\angle HC_2C_3$	123.3	123.9	124.7	122.9	124.1	123.8
$\angle C_2C_3O_2$	178.7	178.9	180.0	179.8	179.3	177.6
$\tau O_1C_1C_2C_3$	0.0	0.0	2.7	0.0	0.0	0.0
			s-E Conformer			
$r(C_1-O_1)$	1.226	1.229	1.226	1.218	1.221	1.241
$r(R-C_1)$	1.109	1.513	1.385	1.368	1.804	1.922
$r(C_1-C_2)$	1.459	1.472	1.478	1.456	1.460	1.465
$r(C_2-C_3)$	1.332	1.329	1.327	1.331	1.331	1.333
$r(C_2-H)$	1.084	1.084	1.082	1.081	1.084	1.086
$r(C_3-O_2)$	1.173	1.175	1.176	1.172	1.172	1.173
$\angle RC_1O_1$	121.2	122.1	122.8	123.1	122.2	115.9
$\angle O_1C_1C_2$	123.2	120.3	122.0	125.5	122.5	119.9
$\angle C_1C_2C_3$	119.9	122.0	121.5	120.3	123.2	122.7
$\angle HC_2C_3$	120.8	119.5	118.9	120.2	118.4	119.3
$\angle C_2C_3O_2$	178.3	178.8	179.1	179.6	179.9	179.9
$\tau O_1C_1C_2C_3$	180.0	180.0	156.5	180.0	180.0	180.0
			E/Z Rotational Transition Structure			
$r(C_1-O_1)$	1.219	1.222	1.225	1.216	1.217	1.228
$r(R-C_1)$	1.105	1.506	1.361	1.356	1.777	1.922
$r(C_1-C_2)$	1.506	1.518	1.513	1.493	1.502	1.524
$r(C_2-C_3)$	1.319	1.318	1.320	1.320	1.321	1.319
$r(C_2-H)$	1.084	1.084	1.084	1.093	1.084	1.084
$r(C_3-O_2)$	1.179	1.181	1.180	1.178	1.178	1.180
$\angle RC_1O_1$	120.7	123.0	123.5	123.1	123.9	123.0
$\angle O_1C_1C_2$	123.5	121.4	123.7	125.7	124.4	121.0
$\angle C_1C_2C_3$	121.0	121.0	119.9	120.7	120.4	120.7
$\angle HC_2C_3$	119.9	119.7	120.1	120.0	119.8	119.5
$\angle C_2C_3O_2$	179.0	178.7	179.4	179.9	179.4	178.2
$\tau O_1C_1C_2C_3$	89.9	88.4	83.3	89.6	86.5	89.3
			1,3-Migration Transition Structure			
$r(C_1-O_1)$	1.191	1.189	1.190	1.186	1.191	1.188
$r(R-C_1)$	1.430	2.019	1.820	1.717	2.138	2.458
$r(R-C_3)$	1.430	1.963	1.543	1.716	2.133	2.200
$r(C_1-C_2)$	1.395	1.382	1.385	1.388	1.392	1.386
$r(C_2-C_3)$	1.395	1.380	1.412	1.388	1.392	1.390
$r(C_2-H)$	1.084	1.085	1.080	1.079	1.085	1.088
$r(C_3-O_2)$	1.191	1.188	1.212	1.186	1.191	1.204
$\angle RC_1C_2$	87.8	96.9	84.8	89.6	93.0	97.0
$\angle RC_3C_2$	87.8	99.6	95.3	89.6	93.2	109.3
$\angle RC_1O_1$	121.8	116.0	123.2	120.3	122.9	112.3
$\angle O_1C_1C_2$	150.4	147.1	152.0	150.1	144.1	150.8
$\angle C_1C_2C_3$	93.7	99.6	100.7	102.2	109.3	99.9
$\angle HC_2C_3$	133.1	130.1	128.1	128.9	125.3	128.4
$\angle C_2C_3O_2$	150.4	148.4	140.4	150.3	143.9	142.0
$\tau O_1C_1C_2C_3$	180.0	180.0	180.0	180.4	183.1	180.0
$\tau RC_1C_2C_3$	0.0	0.0	0.0	6.5	0.0	4.0

[a] Bond lengths in Å and bond angles in deg. [b] Atom labels are illustrated in Chart 1.

quantum mechanically.[16] The solvent is represented by a continuous dielectric, characterized by a given dielectric constant (ϵ). Geometries were optimized at the HF/6-31G* level with the SCRF model and followed by single-point MP2/6-311+G** calculations to include the effect of electron correlation.

Optimized structural parameters for the equilibrium and transition structures of α-oxo ketenes **1**–**6** are given in Table 1. Calculated total and relatives energies are summarized in Tables 2 and 3, respectively. Dipole moments of *s-Z* and *s-E* conformations of α-oxo ketenes are given in Table 4. Calculated energies related to solvent-effect calculations are presented in Table 5. Harmonic vibrational frequencies and infrared intensities of formylketene (**1**) calculated at the HF/6-31G* and MP2/6-31G* levels are collected in Table 6. Finally, the vibrational frequencies and infrared intensities of the C=O and C=C=O vibrations of α-oxo ketenes are given in Table 7. HF/6-31G* vibrational frequencies of *s-Z* and *s-E* conformations of α-oxoketenes (Table VIII) as well as the HF/6-31G* geometries, in *Z*-matrix format (Table IX), for all systems are available as supplementary material.

Discussion

***E/Z* Isomerism.** There are two possible conformations of α-oxo ketenes: *s-Z* and *s-E*. In general, α-oxo ketenes are formed as mixtures of the two isomers.[1,2] However, for sterically hindered α-oxo ketenes, e.g., dipivaloylketene,[1f] only the *s-E* conformation can be observed. The conformational preference is found to be an important factor in governing the reactivity of α-oxo ketenes.[1,2a] Here we have examined the *E/Z* energy differences as well as the rotational barriers of a series of acyl-substituted α-oxo ketenes. The *E/Z* isomerism of several substituted α-oxo ketenes has recently been studied with the semiempirical methods.[17] The bulkiness and electronic nature of the substituent were found to be important in determining the conformational preferences in α-oxoketenes.[1,2a,17]

The calculated *E/Z* energy differences for the series of acyl-substituted α-oxo ketenes are rather small, −2 to +7 kJ mol^{-1} (Table 3). A greater stability of the *s-E* isomer is predicted for compounds **1**, **2**, **4**, and **7**, while the *s-Z* conformation is preferred for the others. It is important to note that both theory and experiment have indicated that bulky substituents on both acyl and ketenic functional groups lead to a preference for the *s-E* conformation.[1,17] Except for compounds **3**, **9**, and **10**, all the optimized equilibrium geometries have a planar structure (Table 1). The *s-E* rotamers of **9** and **10** deviate significantly from planarity; $\tau O_1C_1C_2C_3$ = 151.1 and 162.4° for **9E** and **10E**, respectively (HF/6-31G*).

The *E*- and *Z*-conformers are connected by the transition structure for rotation ($\tau O_1C_1C_2C_3 \approx 90°$, Table 1). Except for $N(CH_3)_2$ (**9**) and C_6H_5 (**10**) substituents, the calculated rotational barriers are of the order of 30–40 kJ mol^{-1}, with small variations. Thus, the two conformers should exist in equilibrium. This result is consistent with the experimental observations of both conformers which exist in equilibrium for several acyl-substituted α-oxo ketenes.[1] Since **9** and **10** have nonplanar *Z*- and *E*-conformations, it is not surprising that these compounds have a rather high degree of flexibility, reflected in their low rotational barriers. It is interesting to note that the rotational barriers calculated at the MP3/6-311+G** level are fairly close to our best estimates [QCISD(T)/6-311+G(2d,p)] (Table 3).

As seen in Table 4, the calculated dipole moments of the *s-Z* conformers are larger than for the corresponding *s-E* conformers (by ~1.5 D). The difference in dipole moment results from the different orientations of the CO

(16) Wong, M. W.; Keith, T. A.; Wiberg, K. B.; Frisch, M. J. *J. Comput. Chem.*, submitted.

(17) Fabian, W. M. F.; Janoschek, R.; Kollenz, G.; Kappe, C. O. *J. Comput. Chem.* **1994**, *15*, 132.

Table 2. Calculated Total Energies[a] (Hartrees) and Zero-Point Vibrational Energies (ZPVE, kJ mol^{-1}) of α-Oxo Ketenes and Related Species

species	total energy			ZPVE
	MP2/6-31G*	QCISD(T)/6-31G*	MP2/6-311+G(2d,p)	
1Z	−265.177 84	−265.221 77	−265.372 89	122.8
1E	−265.177 01	−265.221 47	−265.372 90	122.3
1 *E/Z* TS	−265.157 92	−265.204 15	−265.353 78	119.8
1 1,3-migration TS	−265.116 23	−265.156 68	−265.317 69	109.7
1 1,2-H shift TS	−265.038 18	−265.096 78	−265.236 28	109.5
c-OCCH$_2$CO	−265.109 14	−265.155 75	−265.298 60	118.6
2Z	−304.354 99	−304.414 82	−304.587 20	200.6
2E	−304.353 50	−304.413 95	−304.586 50	200.2
2 *E/Z* TS	−304.336 93	−304.398 69	−304.569 68	198.4
2 1,3-migration TS	−304.272 71	−304.327 58	−304.511 32	193.0
3Z	−320.396 30	−320.449 59	−320.640 89	171.7
3E	−320.393 85	−320.447 65	−320.638 67	172.2
3 *E/Z* TS	−320.384 54	−320.438 73	−320.629 41	169.9
3 1,3-migration TS	−320.371 14	−320.422 34	−320.614 59	173.1
4-membered ring	−320.371 48	−320.422 46	−320.614 70	175.1
4Z	−340.245 64	−340.292 79	−340.504 78	139.4
4E	−340.245 92	−340.293 24	−340.505 22	139.0
4 *E/Z* TS	−340.228 04	−340.276 80	−340.487 58	137.3
4 1,3-migration TS	−340.203 99	−340.247 32	−340.463 94	133.7
5Z	−662.822 35	−662.881 65	−663.070 85	122.8
5E	−662.820 05	−662.879 69	−663.069 11	121.9
5 *E/Z* TS	−662.806 69	−662.867 67	−663.055 59	121.0
5 1,3-migration TS	−662.798 21	−662.853 91	−663.054 16	118.5
6Z	−555.329 48	−555.392 82	−555.579 51	164.9
6E	−555.328 01	−555.392 06	−555.578 68	164.6
6 *E/Z* TS	−555.310 72	−555.376 39	−555.561 05	162.1
6 1,3-migration TS	−555.281 65	−555.341 73	−555.534 69	159.4
OCCHCO•	−264.540 47	−264.583 00	−264.727 01	87.4
SiH_3	−290.674 53	−290.698 58	−290.735 67	67.8
CH_3	−39.668 75	−39.691 04	−39.715 94	81.3
NH_2	−55.690 86	−55.711 55	−55.748 59	54.0
OH	−75.521 03	−75.537 17	−75.594 44	23.9
SH	−398.161 94	−398.184 59	−398.221 72	17.4
H	−0.498 23	−0.498 23	−0.499 81	0.0

[a] Based on MP2(full)/6-31G* geometry. [b] HF/6-31G* values.

Table 3. Calculated Relative Energies[a] (kJ mol^{-1}) for α-Oxo Ketenes

R	relative energy			
	s-Z	*s-E*	*E/Z* TS	1,3-shift TS
H (**1**)	0 (0)	−1.9 (−0.7)	41.4 (41.1)	142.0 (168.5)
CH_3 (**2**)	0 (0)	−0.1 (2.5)	38.9 (38.8)	205.3 (236.9)
NH_2 (**3**)	0 (0)	4.9 (6.5)	26.1 (27.5)	75.9 (89.2)
OH (**4**)	0 (0)	−1.9 (−1.2)	39.0 (40.2)	112.1 (137.4)
SH (**5**)	0 (0)	2.8 (6.5)	34.0 (32.7)	49.3 (79.5)
SiH_3 (**6**)	0 (0)	0.1 (2.9)	39.8 (37.2)	121.3 (157.6)
OCH_3 (**7**)	0 (0)	(−1.4)	(37.9)	(119.2)
SCH33 (**8**)	0 (0)	(5.7)	(30.5)	(71.6)
$N(CH_3)_2$ (**9**)	0 (0)	(9.0)	(24.1)	(45.2)
C_6H_5 (**10**)	0 (0)	(2.8)	(14.1)	(190.0)

[a] QCISD(T)/6-311+G(2d,p)+ZPVE values, with MP3/6-311+G**//HF/6-31G*+ZPVE values in parentheses. [b] Relative to *s-Z* conformation.

Table 4. Calculated[a] Dipole Moments (μ, D) of α-Oxo Ketenes

R	*s-Z*	*s-E*
H (**1**)	3.62	2.41
CH_3 (**2**)	3.84	2.18
NH_2 (**3**)	4.68	2.79
OH (**4**)	2.39	1.12
SH (**5**)	2.35	1.26
SiH_3 (**6**)	3.41	1.85
OCH_3 (**7**)	2.72	1.23
SCH_3 (**8**)	2.00	0.52
$N(CH_3)_2$ (**9**)	4.82	2.93
C_6H_5 (**10**)	4.06	2.51

[a] HF/6-31G* values.

and CCO group dipoles: in the *s-E* conformer, they are opposed, whereas in the *s-Z* conformer they are additive. Thus, the dipole moment difference may be used for a distinction between *s-Z* and *s-E* conformers. In addition, one would expect a differential stabilization effect in solution, in favor of the more polar *s-Z* conformer. We have investigated the solvent effect on the *E/Z* energy difference for formylketene (**1**), acetylketene (**2**), and carboxylketene (**4**) using self-consistent reaction field (SCRF) theory and the spherical cavity approximation.[15] In going from the gas phase ($\epsilon = 1$) to a polar medium of $\epsilon = 40$, the *E/Z* energy differences (at the MP2/6-311+G**//HF/6-31G* level) of **1**, **2**, and **4** increase by 3.6, 4.0, and 2.0 kJ mol^{-1}, respectively (Table 5). In other words, *there is a reversal of the conformational preference in solution*. Hence, we predict that the *s-Z* conformers of the α-oxo ketenes considered here (**1**−**10**) are the dominant forms in solution.

Infrared Spectra. Low-temperature IR spectroscopy represents the most important experimental techniques to study α-oxo ketenes.[1,2] To facilitate further characterization, the infrared spectra of all 10 α-oxo ketenes, calculated at the HF/6-31G* level, are reported in the supplementary material (Table IX). For the parent compound, formylketene (**1**), we have also calculated the IR spectra at the MP2/6-31G* level. A previous study on the cumulenes RN=C=C=C=O has shown that incorporation of electron correlation is essential for the correct prediction of the relative intensities of cumulenic stretching frequencies.[18] As can be seen in Table 6, the

(18) Mosandl, T.; Stadtmüller, S.; Wong, M. W.; Wentrup, C. *J. Phys. Chem.* **1994**, *98*, 1080.

Table 5. Calculated[a] Total Energies (Hartrees) and $\Delta\Delta E$ (kJ mol^{-1}) Related to *E/Z* Energy Differences in the Gas Phase (ϵ = 1) and in Solution (ϵ = 40)

R	$\epsilon = 1$		$\epsilon = 40$[b]		
	s-Z	*s-E*	*s-Z*	*s-E*	$\Delta\Delta E$[c]
H (**1**)	−265.315 78	−265.315 97	−265.319 41	−265.318 22	3.62
CH_3 (**2**)	−304.522 17	−304.520 91	−304.525 24	−304.522 47	3.96
OH (**4**)	−340.429 96	−340.430 40	−340.431 18	−340.430 84	2.02

[a] MP2/6-311+G**//HF/6-31G* values. [b] SCRF calculations (a_0 for R = H, CH_3 and OH are 3.50, 3.75, and 3.70 Å, respectively). [c] Change of *E/Z* energy difference in going from the gas phase (ϵ = 1) to a dielectric medium of ϵ = 40.

Table 6. Calculated IR Spectra Data for Formylketene (1)

mode		frequency (cm^{-1})		intensity (km mol^{-1})	
		HF/6-31G*	MP2/6-31G*	HF/6-31G*	MP2/6-31G*
		(*s-Z*)-Formylketene (**1Z**)			
A′	ν_1	3417	3291	8	14
	ν_2	3204	3024	107	112
	ν_3	2392	2235	1130	580
	ν_4	1961	1745	353	184
	ν_5	1555	1451	24	3
	ν_6	1526	1431	254	201
	ν_7	1218	1139	16	3
	ν_8	1036	989	39	40
	ν_9	872	806	56	33
	ν_{10}	520	460	18	6
	ν_{11}	164	146	4	3
A″	ν_{12}	1139	1014	11	1
	ν_{13}	675	585	91	16
	ν_{14}	611	539	28	67
	ν_{15}	241	228	9	7
		(*s-E*)-Formylketene (**1E**)			
A′	ν_1	3411	3281	16	23
	ν_2	3168	2989	86	87
	ν_3	2380	2228	1171	622
	ν_4	1986	1758	644	309
	ν_5	1596	1483	22	9
	ν_6	1465	1359	36	45
	ν_7	1218	1160	82	104
	ν_8	1199	1119	94	31
	ν_9	677	617	6	5
	ν_{10}	537	499	14	13
	ν_{11}	190	167	19	10
A″	ν_{12}	1127	1011	8	1
	ν_{13}	693	619	99	60
	ν_{14}	630	552	19	27
	ν_{15}	166	153	13	6

MP2 relative intensities are similar to those calculated at the Hartree–Fock level. This lends confidence to our predicted HF infrared intensities for other systems (**2**–**9**). Note that the MP2 C=O stretching frequencies (ν_4) are significantly different from the HF values. Indeed, the calculated HF frequencies are 16–17% higher than the experimental values,[1g] 1678 (**1Z**) and 1707 (**1E**) cm^{-1}. For acetylketene (**2**), the Hartree–Fock $\nu_{C=O}$ are also overestimated by a similar magnitude (calculated 1960 (**2Z**) and 1984 (**2E**) cm^{-1}; experimental[1e] 1681 (**2Z**) and 1698 (**2E**) cm^{-1}). This suggests that a scaling factor of 0.86, instead of the standard value (0.8929),[12] should be used for reliable prediction of carbonyl stretching frequencies in α-oxoketenes.

The characteristic features of the IR spectra of the α-oxo ketenes are the strong absorption bands due to the carbonyl (C=O) and ketenic (C=C=O) stretching vibrations. In particular, the experimental distinction between *s-Z* and *s-E* conformers is based on the frequency difference and intensity ratio for these two vibrational modes.[1e] As is evident in Table 6, the *s-Z* conformers are calculated to have higher frequency (by 5–20 cm^{-1}) but less intense ketenic stretching vibration than the corresponding *s-E* rotamers. On the other hand, the *s-Z* conformers are predicted to have a lower frequency (by 13–38 cm^{-1}) but more intense carbonyl band. In all cases, the carbonyl absorption peaks of the *s-E* conformers are about twice as intense as in the *s-Z* forms. Hence, our calculated results are in excellent agreement with the experimental findings for the C=O and C=C=O vibrations of α-oxo ketenes:[1] the frequency separation is larger for the *s-Z* than the *s-E* forms, and the intensity ratio of the two bands is larger for *s-E*. Experimental C=C=O stretching frequencies are available for compounds **1**, **2**, **7**, and **10**: 2145 (**1Z**),[1g] 2142 (**1E**);[1g] 2143 (**2Z**),[1e] 2133 (**2E**);[1e] 2143 (**7Z**),[1a] 2132 (**7E**);[1a] 2143 (**10Z**),[1c] and 2134 (**10E**)[1c] cm^{-1}. The observed data are in good accord with our calculated values (Table 7).

Table 7. Calculated[a] Vibrational Frequencies[b] and Infrared Intensities[c] C=O and C=C=O Stretching Vibrations of α-Oxo Ketenes

R	mode	*s-Z*	*s-E*
H (**1**)	$\nu_{C=O}$	1686 (353)	1708 (644)
	$\nu_{C=C=O}$	2136 (1130)	2125 (1171)
CH_3 (**2**)	$\nu_{C=O}$	1686 (265)	1706 (536)
	$\nu_{C=C=O}$	2133 (1195)	2119 (1127)
NH_2 (**3**)	$\nu_{C=O}$	1664 (381)	1701 (686)
	$\nu_{C=C=O}$	2141 (1152)	2121 (1092)
OH (**4**)	$\nu_{C=O}$	1703 (439)	1735 (874)
	$\nu_{C=C=O}$	2146 (1113)	2140 (1102)
SH (**5**)	$\nu_{C=O}$	1666 (301)	1688 (625)
	$\nu_{C=C=O}$	2142 (1332)	2132 (1124)
SiH_3 (**6**)	$\nu_{C=O}$	1623 (195)	1635 (430)
	$\nu_{C=C=O}$	2124 (862)	2110 (628)
OCH_3 (**7**)	$\nu_{C=O}$	1686 (332)	1717 (702)
	$\nu_{C=C=O}$	2141 (1173)	2136 (1117)
SCH_3 (**8**)	$\nu_{C=O}$	1649 (254)	1672 (544)
	$\nu_{C=C=O}$	2138 (1407)	2129 (1160)
$N(CH_3)_2$ (**9**)	$\nu_{C=O}$	1615 (360)	1650 (615)
	$\nu_{C=C=O}$	2136 (1294)	2117 (1073)
C_6H_5 (**10**)	$\nu_{C=O}$	1650 (227)	1679 (506)
	$\nu_{C=C=O}$	2132 (1545)	2118 (1082)

[a] HF/6-31G* values; for the full spectra, see the supplementary material. [b] Scaled by 0.8929 and 0.86 (see text) for the C=C=O and C=O stretching frequencies, respectively (in cm^{-1}). [c] Intensity values (in km mol^{-1}) are parentheses.

1,3-Migration. There are three plausible routes for the 1,3-migration process in α-oxo ketenes: (1) cleavage of the C–R bond and recombination, (2) two successive 1,2-R shifts, and (3) a direct 1,3-R shift. For compounds **1**–**6**, the dissociation energies (to R$^\bullet$ + OCCHCO$^\bullet$) are quite substantial, 355, 337, 386, 426, 289, and 289 kJ mol^{-1}, respectively. We have examined the 1,2-R shift pathway for formylketene (**1**). This reaction pathway involves a three-membered cyclic transition structure and a cyclic intermediate OCCH$_2$CO, lying 310 and 167 kJ mol^{-1}, respectively, above formylketene. For comparison, route 3, a direct 1,3-hydrogen shift via a four-centered cyclic transition structure, requires a significantly lower activation barrier of 142 kJ mol^{-1}. Hence, we may conclude that the concerted 1,3-R shift is the most favorable route for 1,3-migration in α-oxo ketenes.

Since the larger systems (**7**–**10**) were investigated with the MP3/6-311+G** level of theory, it is instructive to

compare the MP3 activation energies, for compounds **1**–**6**, with our best estimates [QCISD(T)/6-311+G(2d,p)]. As seen in Table 3, the MP3 barriers are significantly too high compared to the QCISD(T) estimates. The differences, however, are rather uniform, the MP3 values being lower by 20–30 kJ mol^{-1}. Thus, it may be reasonable to assume that the change from MP3 to QCISD(T) is of the order −25 kJ mol^{-1}, and one may apply this empirical correction to the MP3 barriers to obtain a pseudo QCISD(T) estimate. In addition, the good correlation between the MP3 and QCISD(T) values suggests that the MP3 level should be reliable for qualitative prediction of the trend in 1,3-migration barriers in α-oxo ketenes.

The 1,3-hydrogen shift of the parent compound, formylketene (**1**), has been studied by Nguyen, Ha, and More O'Ferrall.[9] Using the MP4SDQ/6-31G** theory, they found that the 1,3-migration requires an activation barrier of 166 kJ mol^{-1}. Our higher-level calculations [QCISD(T)/6-311+G(2d,p)] predict a somewhat smaller barrier of 142 kJ mol^{-1}. This is readily confirmed by calculations at the G2(MP2) level of theory,[11] which also predicts a barrier of 142 kJ mol^{-1}. This result is rather surprising since 1,3-sigmatropic shifts in neutral molecules usually require large activation energies.[18–20] For instance, 1,3-hydrogen shifts in HN=C=C=C=O, HN=C=C=O, and HN=C=C=S are calculated to have substantial barriers of 300–400 kJ mol^{-1}.[18,19b] It is of interest to note that 1,3-hydrogen shifts in HCOOH, HCOSH, and HCSSH are also predicted to have relatively low barriers (137, 136, and 110 kJ mol^{-1}, respectively, at the MP4SDQ/6-31G** level).[21]

Let us first consider the effect of several simple substituents, CH_3 (**2**), NH_2 (**3**), OH (**4**), SH (**5**), and SiH_3 (**6**), on the calculated barrier height. The calculated results (Table 3) illustrate that substitution of an electron rich group (**3**–**5**), with an unshared pair of electrons, for hydrogen decreases the activation barrier. On the other hand, a significant destabilizing effect is calculated for a methyl substituent (**2**). Silyl substitution (**6**) is predicted to cause a slightly lower barrier than for formylketene (**1**). For the SH (**5**) substituent, the calculated barrier is just 45 kJ mol^{-1}, 93 kJ mol^{-1} less than that of formylketene. What is the origin of the dramatic rate acceleration by electron rich substituent in oxoketene-oxoketene rearrangement?

The direct 1,3-R shift involves an interaction between the R group and the carbon atom (C_3) of the ketene moiety in the four-centered transition structure (Chart 1). Inspection of the lowest unoccupied molecular orbital (LUMO) of *s-E* α-oxo ketenes indicates that there is a vacant atomic p orbital (with the largest coefficient) at the C_3 atom in the molecular plane (Figure 1a). Thus, one would expect *n*-electron donor substituents (**3**–**5**) to interact strongly with the vacant p orbital and thus stabilize the 1,3-migration transition structures. This orbital interaction is symmetry allowed. The donor–acceptor interaction between the lone pair electrons of an amino group and the ketene acceptor orbital in **3** is illustrated in Figure 1b. Since the 1,3-shift transition structure (Chart 1) involves a partially broken C_1–R bond, the magnitude of the C–R bond dissociation energy could also be a contributing factor influencing the barrier height. This could be one reason why the activation barrier for 1,3-SH migration in **5** is slightly lower than that for the 1,3-NH_2 shift in **3**.

Consistent with the experimental observation,[5] the methyl group (**2**) is calculated to be a poor migrator, and other alkyl groups are expected to behave similarly. There is no lone pair available for a donor–acceptor interaction in this case. Furthermore, a pentacoordinated carbon is required in the 1,3-migration transition structure. As a consequence, the 1,3-methyl shift in α-oxo ketene requires a very substantial barrier of 205 kJ mol^{-1}. Although a silyl group is similar to a methyl group, the calculated barrier for 1,3-silyl migration is significantly less (by 84 kJ mol^{-1}). The lower activation barrier may be explained in part by the well-known electron-donating ability of silicon and in part by the ability of the silicon atom to accept hypervalency.[22] In this case, a complementary interaction between the R group (SiH_3) and the ketene HOMO is also involved. This is reflected in the significant overlap between the 3d AOs of the silicon atom and the 2p AOs of the C_3 atom in the 1,3-migration transition structure.

Our hypothesis of donor–acceptor interaction is further supported by calculations on methyl-substituted *n*-electron donor groups, namely, OCH_3 (**7**), SCH_3 (**8**), and $N(CH_3)_2$ (**9**). Methyl substitution on OH, SH, and NH_2 groups increase their electron-releasing abilities, and thus one would expect an increase in strength of the donor–acceptor interaction. Indeed, the calculated barrier heights for OCH_3 (**7**), SCH_3 (**8**), and $N(CH_3)_2$ (**9**) are significantly less than for the corresponding unsubstituted ones (i.e., OH (**4**), SH (**5**), and NH_2 (**6**), respectively) by 18, 8, and 44 kJ mol^{-1}, respectively. Thus, the predicted order of 1,3-migratory aptitude in α-oxo ketenes is NR'_2 > SR' > OR', where R' = alkyl group. This calculated trend agrees well with experimental findings for the 1,3-migration in thioacyl isocyanates (RCS-N=C=O), isoelectronic analogues of α-oxo ketene (eq 3).[6a]

Applying the MP3–QCISD(T) correction, our best estimates of the activation energies for methylthio (**8**) and dimethylamino (**9**) substituents are 47 and 20 kJ mol^{-1}, respectively. 1,3-Migration reactions for **8** and **9** are, therefore, predicted to be facile processes. This result is in excellent accord with experimental findings for the imine analogues, viz. imidoylketenes: dramatic rate accelerations were observed for SCH_3 and $N(CH_3)_2$ substituents.[4b,c] For the dimethylamino substituent (**9**), a metastable intermediate is found on the reaction profile.[23] However, rearrangement of this cyclic intermediate to the open-chain oxo ketene is associated with

(19) (a) Flammang, R.; Landu, D.; Laurent, S.; Barbieux-Flammang, M.; Wong, M. W.; Kappe, C. O.; Wentrup, C. *J. Am. Chem. Soc.* **1994**, *116*, 2005. (b) Flammang, R.; Van Haverbeke, Y.; Laurent, S.; Barbieux-Flammang, M.; Wong, M. W.; Wentrup, C. *J. Phys. Chem.* **1994**, *98*, 5801. (c) Rodwell, W. R.; Bouma, W. J.; Radom, L. *Int. J. Quantum Chem.* **1980**, *18*, 107. (d) Bernadi, F.; Robb, M. A.; Schlegel, H. B.; Tomachini, G. *J. Am. Chem. Soc.* **1984**, *106*, 1198. (e) Poirier, R. A.; Majlessi, D.; Zielinski, T. J. *J. Comput. Chem.* **1986**, *7*, 464. (f) Hess, B. A., Jr.; Schaad, L. J.; Pancir, J. *J. Am. Chem. Soc.* **1985**, *107*, 149.

(20) A high barrier (300 kJ mol^{-1}) is also calculated for the isomerization of ketenimine (H_2C=C=NH) to acetonitrile (H_3CC≡N): Leung-Toung, R.; Wong, M. W.; Wentrup, C. To be published.

(21) Nguyen, M. T.; Weringa, W. D.; Ha, T.-K. *J. Phys. Chem.* **1989**, *93*, 7956.

(22) For a review, see: Chuit, C.; Corriu, J. P.; Reye, C.; Young, J. C. *Chem. Rev.* **1993**, *93*, 1371.

(23) A stable cyclic intermediate is also calculated for R = NH_2 (**3**) at the MP2/6-31G* level (lying in an energy well of just 1 kJ mol^{-1}). However, at the QCISD(T)/6-311+G(2d,p) level, the cyclic structure rises slightly above the transition structures in energy, suggesting the four-centered equilibrium structure may not be stable at higher levels of theory. No stable four-membered cyclic equilibrium structures are found for compounds **1**, **2**, **4**–**8**, and **10**.

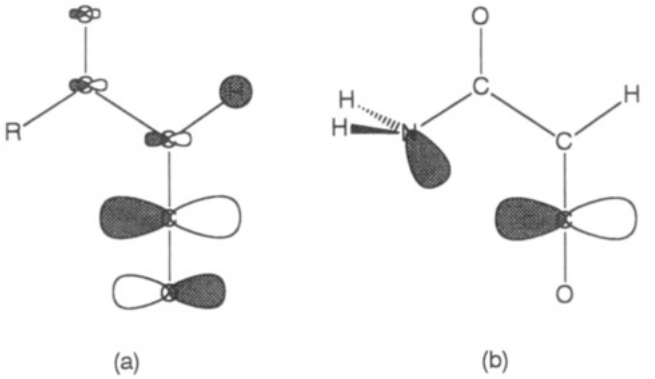

Figure 1. (a) The lowest unoccupied molecular orbtial (LUMO) of *s-E* α-oxo ketenes. (b) The donor−acceptor interaction between the lone pair electrons of an amino group and the vacant carbon p orbital of the ketene LUMO in **3**.

a small barrier of 10 kJ mol^{-1} (MP3/6-311+G**). Hence, direct observation of this cyclic intermediate will not be straightforward.

Finally, we examine the 1,3-phenyl shift in benzoylketene (**10**). The calculated barrier is significantly lower than for acetylketene (**2**), by 47 kJ mol^{-1} (MP3/6-311+G**). The better migrating ability can readily be rationalized by the availability of the HOMO (π orbital) in the (rotated) phenyl group as electron donor. Since π electrons are less effective donors than lone pair electrons, the phenyl migratory aptitude is significantly less than for the *n* substituents, NH_2 (**3**), OH (**4**), and SH (**5**) (Table 3). One should expect donor-substituted phenyl groups to exhibit higher migratory aptitudes. Our best estimate of the activation energy for the 1,3-phenyl shift in benzoylketene is 165 kJ mol^{-1} (based on the MP3-QCISD(T) correction). The calculated result is consistent with the experimental observation that no carbon scrambling occurred under FVP conditions at 400 °C; at 550 °C the 1,3-phenyl migration was ca. 30%, and at 750 °C 100% complete.[3a,4a] This suggests a significant but readily accessible activation energy for the 1,3-phenyl shift. Since the parent compound (**1**) has an activation barrier (142 kJ mol^{-1}) comparable to that of benzoylketene, we predict the 1,3-H shift in formylketene to be an observable process. There are experimental indications of a 1,3-H shift in imidoylketenes.[4b]

In summary, electron rich substituents strongly stabilize the transition structures for 1,3-migration in α-oxo ketenes. The interaction between the R group and the ketene LUMO, in particular the atomic p orbital at C_3 (Figure 1), is the key factor in determining the magnitude of the activation barrier. The reaction profiles for the oxo ketene−oxo ketene rearrangements for compounds **1**, **2**, **7**, **8**, and **9** are summarized in Figure 2. For compounds **1**, **2**, **7**, and **8**, there is only one transition state in going from reactant to product. On the other hand, a stable cyclic intermediate is involved on the reaction profile of **9**. Further studies on this intriguing type of 1,3-migration in other cumulene systems (e.g., vinylketene, imidoylketene, etc.) are underway, and results will be reported in due course.[24]

(24) Wong, M. W.; Wentrup, C. To be published.

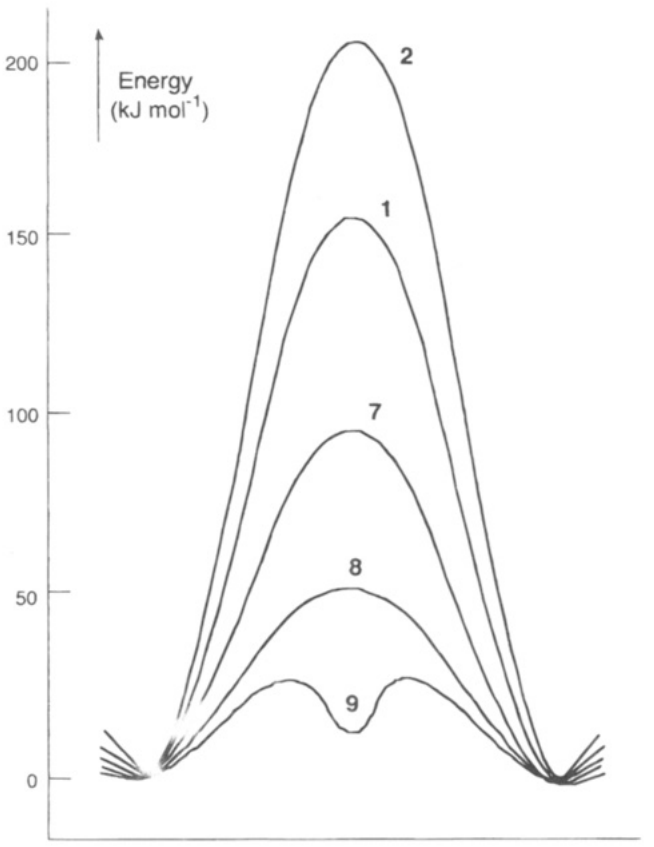

Figure 2. Schematic energy profiles for 1,3-migration in **1**, **2**, **7**, **8**, and **9**.

Conclusions

In this paper we have investigated the reaction mechanism of 1,3-migration in substituted α-oxo ketenes. These α-oxo ketene−α-oxo ketene rearrangements proceed via a four-centered cyclic transition structure. In accordance with the experimental findings, electron rich substituents are found to decrease the activation barriers. The migratory aptitude is in the order $N(CH_3)_2$ > SCH_3 > SH > NH_2 > OCH_3 > OH > SiH_3 > H > C_6H_5 > CH_3. The calculated barriers in the series RCOCH=C=O decrease with the increasing electron releasing ability of R. The effect of substituents on the 1,3-migration barriers can be readily understood in terms of the donor−acceptor interaction between the R substituent and the vacant carbon (C_3) p orbital of the ketene LUMO.

Acknowledgment. We thank the Australian Research Council for financial support and for a Research Fellowship for M.W.W. and the University of Queensland for generous allocation of computer time.

Supplementary Material Available: Tables of HF/6-31G* harmonic vibrational frequencies and optimized geometries for **1**−**10**, in Z-matrix format (13 pages). This material is contained in libraries on microfiche, immediately follows this article in the microfilm version of the journal, and can be ordered from the ACS; see any current masthead page for ordering information.